Sedimentation of a Sphere Near a Vertical Wall in an Oldroyd-B Fluid

P. Singh
Department of Mechanical Engineering
New Jersey Institute of Technology
University Heights
Newark, NJ 07102

D.D. Joseph
Department of Aerospace Engineering and Mechanics
University of Minnesota
Minneapolis, MN 55455

A code based on the distributed Lagrange multiplier/fictitious domain method (DLM) is used to study the motion of a sphere sedimenting in a viscoelastic liquid near a vertical wall. The viscoelastic liquid is assumed to be shear thinning and modeled by a shear-thinning Oldroyd-B model. Our simulations show that when the Deborah number based on the sphere velocity is O(1) and its initial position is sufficiently close to the wall, it moves towards the wall. This tendency of a sedimenting sphere to move closer to the vertical wall is enhanced by shear thinning, and also by an increase in the Deborah number. In a Newtonian liquid, on the other hand, the sphere moves away from the vertical wall and attains a steady position between the channel center and the wall. The sense of rotation of a sedimenting sphere when it is close to the vertical wall, for both Newtonian and viscoelastic liquids, is anomalous, i.e., the sphere rotates as if rolling up the wall. However, when the sphere is away from the wall the direction of rotation reverses. These results are in agreement with the experimental data reported in [1-4]. In two dimensions, on the other hand, simulations show that a sedimenting cylinder moves away from the wall in both Newtonian and viscoelastic liquids. These numerical results prove that the attraction between a wall and a particle sedimenting in a viscoelastic liquid is a three-dimensional effect, i.e., exists for a sphere but not for a cylinder, and it is enhanced by shear thinning.

1. Introduction

It is well known that when a sphere is dropped near a vertical wall in a Newtonian liquid it moves away from the wall as it falls downwards under gravity. On the other hand, when the suspending liquid is viscoelastic and the sphere is released sufficiently close to the wall it moves towards the wall as it falls downwards. This property of viscoelastic fluid-particle systems is of importance in many industrial processes. For example, the quality and durability of paints may depend on the settling property of suspended particulates. Our goal in this paper to use the results of direct numerical simulations to understand the mechanisms that give rise to this drastic difference in the particle trajectories near a wall.

The problem of interaction between a sphere and a wall was first studied by Goldman, Cox and Brenner [5] who found that a sphere falling in a channel filled with a liquid cannot be in contact with the vertical channel walls, as a lubrication layer develops between the wall and the falling sphere. They also found that under certain conditions the sphere falls downwards while rotating in a clockwise direction, as shown in figure 1a [1-5]. This sense of rotation is referred to be anomalous because it is the sense of rotation that exists when a sphere rolls up the wall without slipping. The normal sense of rotation exists when a sphere rotates down an inclined plane and there is no slip at the point of contact, as shown in figure 1b. In other words, the sense of rotation of a sphere falling in a channel filled with a liquid near a vertical wall is the opposite of that in rolling at a wall without slipping. The sense of rotation in a liquid is the opposite of that for normal rolling because as the sphere falls downwards the liquid must go around it, as shown in figure 1a.

When the wall is horizontal or at an angle to the gravity the direction of rotation of a particle depends on the relative magnitudes of the buoyant weight and hydrodynamic forces [3]. When the buoyant weight dominates the particle touches the wall and rotates in a normal manner. On the other hand, when the hydrodynamic forces dominate the sphere is lifted from the wall and it rotates in an anomalous manner. It is interesting to note that it was shown in [2] that the relative magnitudes of buoyant weight and hydrodynamic forces can be adjusted by changing the angle between the gravity and the wall. When this angle is very small, i.e., the wall is approximately vertical, the hydrodynamics force dominates and the particle moves away from the wall and rotates in an anomalous manner. But, when the angle is close to 90 degrees, i.e., the wall is approximately horizontal, the buoyant weight dominates and the

sphere touches the wall and rotates in a normal manner. Clearly, for a given fluid-particle combination there is a critical angle for which the transition from the anomalous rotation to the normal rotation takes place. This critical angle depends on the fluid properties, as well as on the sphere size and density. For a set of fluid-particle combinations these angles are reported in [3].

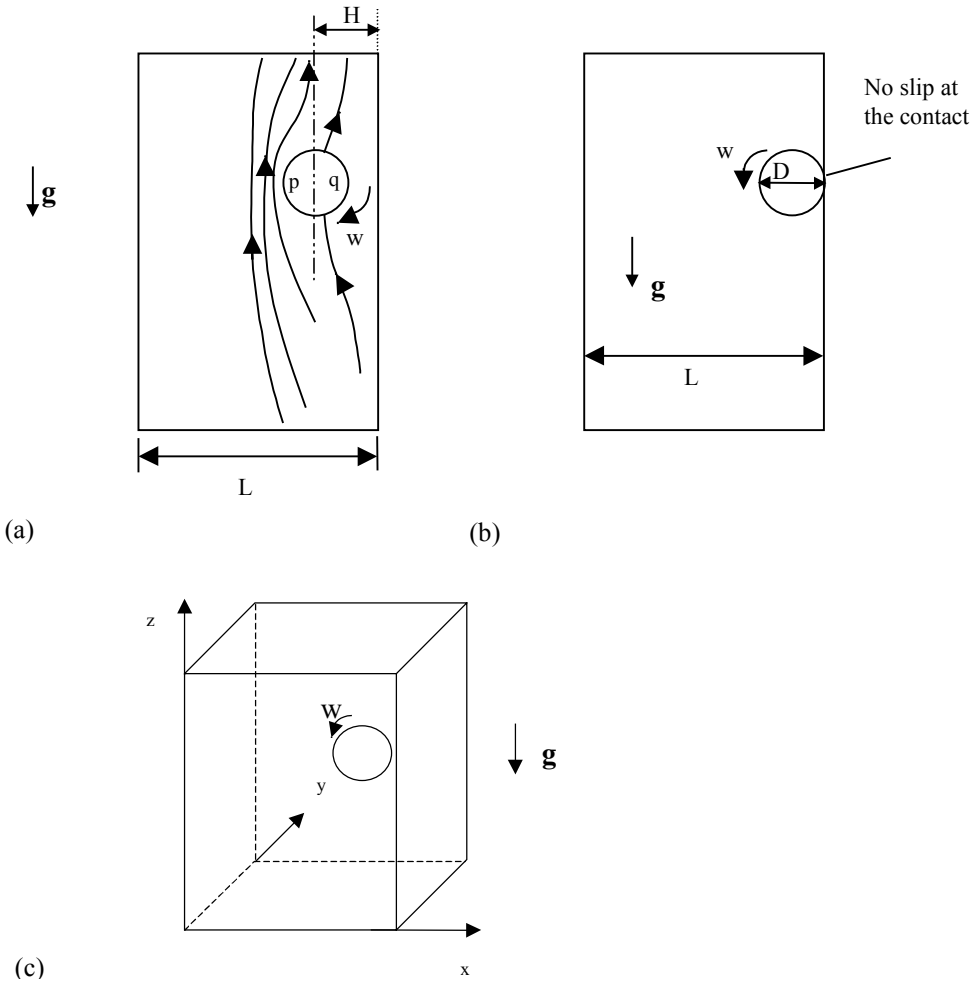

Figure 1. A schematic of a particle sedimenting near a vertical wall. (a) The sense of rotation shown is anomalous, and the streamlines are shown in a frame moving with the particle. (b) A particle rolling on a wall with no slip at the point of contact. The sense of rotation is normal. (c) A particle dropped in a box near the right hand side wall.

Similarly, in a pressure driven flow the sense of rotation of particles near the bottom surface of a horizontal pipe depends on whether or not the particles are lifted up from the lower surface. When the applied pressure gradient is small the particles roll on the pipe

surface and rotate in a normal manner, and when the applied pressure gradient is sufficiently large the particles are lifted up and rotate anomalously.

It is noteworthy that when a rotating particle is placed in a uniform potential flow, i.e., the Reynolds number approaches infinity, a lift force acts on the particle in the direction normal to the uniform flow direction. Specifically, the lift force $\mathbf{L} = \rho \mathbf{U} \times \mathbf{\Gamma}$, where $\mathbf{U}$ is the uniform flow velocity, ρ is the fluid density and $\mathbf{\Gamma}$ is the circulation. For a rotating particle the circulation can be assumed to be equal to the angular velocity $\boldsymbol{\omega}$. The magnitude of lift force therefore is proportional to the magnitudes of uniform flow velocity and rate of rotation. Also note that the anomalous rotation of the particle causes both front and rear stagnation points to shift towards the wall, assuming that they are on the cylinder surface, as shown in figure 1a. Since the velocity on the particle surface away from the wall is greater than on the surface closer to the wall, the pressure on the former surface is smaller than that on the latter surface. Therefore, a net pressure force acts on the particle in the direction away from the wall. Also note that for a particle falling near a wall and rotating in an anomalous manner it is easy to see that the above expression for the lift--in a frame attached to the particle--gives a force which acts in the direction away from the wall.

For a second order fluid it was shown in [6,7] that the elastic contribution to the normal stress on the body surface is equal to $-\Psi_1(0)\dot{\gamma}^2$, where $\Psi_1(0)$ is the first normal stress difference and $\dot{\gamma}$ is the shear rate. Thus, the value of elastic normal stress is maximum at a point where the shear rate is maximum. These elastic normal stresses cause a long body, e.g., an ellipse, to sediment with its major axis parallel to the vertical direction. For a sphere sedimenting near a wall the viscoelastic normal stresses at the points marked p and q, in general, would be different and may result in a net force towards the wall (see figure 1a). For an Oldroyd-B liquid, however, the viscoelastic normal stresses on the body surface are zero, but the shear stresses are nonzero and may result in a net force towards the wall [8].

The motion of a sphere sedimenting in a channel near a vertical wall in an Oldroyd-B liquid depends on the Reynolds number $\mathrm{Re}=\frac{\rho_L U D}{\eta}$, the Deborah number $\mathrm{De}=\frac{U\lambda_r}{D}$, the shear thinning nature of the viscoelastic liquid, the channel blockage ratio D/L, the ratio of particle and liquid densities, and the dimensionless distance from the wall h. Here λ_r is the relaxation time of the fluid, η is the zero shear viscosity of the fluid, U is the particle sedimentation

velocity, D is the particle diameter, h=H/D, H is the distance from the wall, ρ_L is the liquid density, and L is the channel width. The particle velocity U depends on its buoyant weight and the liquid properties. It also depends on the distance from the wall h; the sedimentation velocity decreases as the sphere approaches the wall. It is useful to define the Mach number $M=\sqrt{\mathrm{Re\ De}}$ and the elasticity number $E=\frac{De}{Re}$.

There are several analytical studies that have investigated the role of inertia, viscoelasticity and shear thinning on the motion of a sphere sedimenting near a vertical wall. The results of these past studies have been summarized in Becker, McKinley and Stone [4]. They have also studied the role of weak viscoelastic effects using a second order fluid and weak inertial effects up to first order in Reynolds number on the motion of a sedimenting sphere in three dimensions. These studies have concluded that when the Reynolds number is zero and the liquid is Newtonian the sphere sediments parallel to the wall and undergoes normal rotation, i.e., rotates as if rolling down the wall. The weak viscoelastic effects cause the particle to move away from the wall and also lead to an increase in the drag, i.e., the sedimentation velocity is smaller in the viscoelastic liquid. The shear thinning decreases the angular velocity of the sphere. The inertial forces cause the sphere to move away from the wall. Becker et al. also did experiments that are in agreement with the results reported in [1,2]. They concluded that the presence of weak viscoelasticity, inertia or shear thinning could not explain the experimental observations that a sphere sedimenting in a viscoelastic moves towards the wall and that it rotates anomalously. They also noted that this is probably due to the fact that the Deborah number in experiments is of order one and suggested that direct numerical simulations in three-dimensions should be performed to understand the motion of a sphere at these Deborah numbers.

The interaction of a particle and a wall for a Newtonian fluid in a two dimensional channel was first simulated in [3] by using the arbitrary Eulerian Lagrangian approach. Specifically, the authors simulated the transient motion of a cylindrical particle sedimenting near a vertical wall. These simulations reproduced the qualitative features that in a Newtonian liquid the particle drifts away from the wall and that when it is close to the wall the sense of rotation is anomalous, but when it is away from the wall it rotates in a normal manner. They

also found that the particles sideways drift velocity and the rotation rate decrease with increasing distance from the wall.

The motion of cylindrical particles sedimenting near a vertical wall in an Oldroyd-B fluid in two dimensions was first simulated by Feng, Huang and Joseph [8] by using the arbitrary Eulerian Lagrangian approach (also see [9-11]). These authors have found that in a Newtonian liquid the force acting on a particle near a wall is away from the wall. In an Oldroyd-B liquid they found that there is a critical value of the dimensionless distance h from the wall for which the hydrodynamic force acting on the particle in the direction normal to the wall is zero. When h is less than this critical value the force is repulsive, and when h is greater than the critical value the force is attractive. Therefore, for a particle sedimenting in an Oldroyd-B fluid in two-dimensions the stable position is away from the wall. When the Deborah number is of order one the critical value of distance is O(D). The exact value of the critical distance depends on the Reynolds number, the Deborah number, and the ratio D/L. These two dimensional simulations, therefore, could not explain the experimental observations that a sphere sedimenting near a wall in a viscoelastic liquid moves towards the wall. The magnitude of both repulsive and attractive forces was found to increase with increasing Deborah number. They also found that the torque acting on a fixed particle near the wall is in the anomalous direction, i.e., if the particle is allowed to rotate freely, it would rotate in an anomalous manner. But, of course, when the particle is allowed to rotate freely the velocity and stress distributions would also change. In their paper they did not report the direction of rotation of a freely sedimenting particle.

Binous and Phillips [12] numerically studied the motion of a sphere sedimenting in a suspension of finite-extension-nonlinear-elastic (FENE) dumbbells. In their calculations the fluid was assumed to be Stokesian, and the interactions among the particles and the dumbbells was modeled using well-known relations from low Reynolds number hydrodynamics. Their numerical results show that the presence of FENE dumbbells have a strong effect on the motion of sphere. In particular, they found that a sphere sedimenting near a wall in a suspension of FENE dumbbells rotates in an anomalous manner and that when the initial position of the sphere is less than ~6D from the wall it moves towards the wall. The range of wall attraction in experiments is about ~1.5D. They also found that the distance between the sphere and the wall decreases approximately linearly with time which is in good agreement

with the experimental data reported in [1-4]. They also found that the sense of rotation becomes normal when the distance between the sphere center and the wall is less than ~D. In experiments, on the other hand, the rotation remains anomalous.

Our goal in this paper is to use a code based on the distributed Lagrange multiplier/fictitious domain method (DLM) [13-15] to simulate the motion of a rigid sphere suspended in a shear thinning Oldroyd-B fluid and to understand the forces that move the sphere closer to the wall. One of the key features of our DLM method is that the fluid-particle system is treated implicitly by using a combined weak formulation where the forces and moments between the particles and fluid cancel, as they are internal to the combined system. These internal hydrodynamic forces are not needed for determining the motion of particles. In our combined weak formulation we solve fluid flow equations everywhere in the domain, including inside the particles. The flow inside the particles is forced to be a rigid body motion using the distributed Lagrange multiplier method. This multiplier represents the additional body force per unit volume needed to maintain rigid-body motion inside the particle boundary, and is analogous to the pressure in incompressible fluid flow, whose gradient is the force needed to maintain the constraint of incompressibility.

In our numerical method the Marchuk-Yanenko operator splitting technique is used to decouple the difficulties associated with the incompressibility constraint, the nonlinear convection term, the viscoelastic term and the rigid body motion constraint. This gives rise to the four sub-problems that are solved using matrix-free algorithms. The code is verified by comparing the time dependent velocity and position of a sedimenting sphere in a box for two different mesh refinements, and for two different time steps. It is shown that the results are independent of the mesh resolution and the time step.

We find good agreement between the numerically computed trajectories of a sphere sedimenting near a vertical wall in a channel and the experimental observations reported in [1-4]. In particular, when the Deborah number is O(1) and the initial position of the sphere is sufficiently close to the vertical wall, it moves closer to the wall as it falls downwards. This tendency of a sedimenting sphere to move closer to the nearby vertical wall is enhanced by shear thinning as well as by an increase in De. In a Newtonian liquid, on the other hand, the sphere moves away from the vertical wall and attains a steady state position somewhere between the channel wall and the channel center. In a two dimensional channel, for both

Newtonian and viscoelastic liquids, the particle moves away from the wall to a stable position that is between the channel wall and the channel center. When De is O(1) the stable position may be only O(D) away from the wall. The direction of rotation of a sphere when it is close to the vertical wall, in both Newtonian and viscoelastic liquids, is anomalous, i.e., the sphere rotates as if rolling up the wall. But, when the sphere is away from the wall the direction of rotation reverses.

The outline of this paper is as follows. In the next section we will state the governing equations for the shear thinning Oldroyd-B model and for the motion of a sedimenting particle, and briefly describe our numerical method. In section 3, we will discuss the convergence study that shows that the numerical results are independent of the mesh size as well as the time step. We will also discuss the results obtained in two and three dimensions for a particle sedimenting near a wall in Newtonian and Oldroyd-B liquids.

2. Problem statement and numerical method

The viscoelastic fluid is modeled via the shear-thinning Oldroyd-B model. In this paper we will present results for both two- and three-dimensions. The computational domain Ω is assumed to be rectangular in two dimensions and box shaped in three dimension. The domain boundary is denoted by Γ, and the interior of a particle by P(t). The upstream part of Γ will be denoted by Γ^-. The governing equations for the fluid-particle system are:

$$\rho_L \left[\frac{\partial \mathbf{u}}{\partial t} + \mathbf{u}.\nabla \mathbf{u} \right] = \rho_L \mathbf{g} - \nabla p + \nabla.\boldsymbol{\sigma} \qquad \text{in } \Omega \backslash \overline{P(t)} \qquad (1)$$

$$\nabla \cdot \mathbf{u} = 0 \qquad \text{in } \Omega \backslash \overline{P(t)} \qquad (2)$$

$$\mathbf{u} = \mathbf{u}_L \qquad \text{on } \Gamma \qquad (3)$$

$$\mathbf{u} = \mathbf{U} + \omega \times \mathbf{r} \qquad \text{on } \partial P(t) \qquad (4)$$

with the evolution of the configuration tensor **A** given by

$$\frac{\partial \mathbf{A}}{\partial t} + \mathbf{u}.\nabla \mathbf{A} = \mathbf{A}.\nabla \mathbf{u} + \nabla \mathbf{u}^T.\mathbf{A} - \frac{1}{\lambda_r}(\mathbf{A} - \mathbf{I}), \qquad (5)$$

$$\mathbf{A} = \mathbf{A}_L \qquad \text{on } \Gamma^-.$$

Here **u** is the velocity, p is the pressure, the extra stress tensor $\boldsymbol{\sigma} = \frac{c\eta_s}{\lambda_r}\mathbf{A} + 2\eta_s \mathbf{D}$, ρ_L is the density, **D** is the symmetric part of the velocity gradient tensor, c is a measure of polymer

concentration in terms of the zero shear viscosity, and λ_r is the relaxation time. The fluid viscosity $\eta = \eta_s + \eta_p$, where $\eta_p = c\,\eta_s$ is the polymer contribution to viscosity and η_s is the purely viscous contribution to viscosity. The fluid retardation time is equal to $\frac{\lambda_r}{1+c}$. Shear thinning is incorporated into the Oldroyd-B model by assuming that the total viscosity varies according to the Carreau-Bird law:

$$\frac{\eta - \eta_\infty}{\eta_0 - \eta_\infty} = \left[1 + (\lambda_3 \dot{\gamma})^2\right]^{\frac{n-1}{2}}.$$

Here $\dot{\gamma}$ is the strain rate defined in terms of the second invariant of the symmetric part of the velocity gradient tensor

$$\dot{\gamma} = \sqrt{2\mathbf{D}:\mathbf{D}} = \sqrt{2(D_{11}^2 + D_{22}^2 + D_{33}^2 + 2D_{12}^2 + 2D_{23}^2 + 2D_{13}^2)},$$

where D_{ij} is the ij-component of $\mathbf{D}$, η_0 is the zero shear viscosity, η_∞ is the minimum value of viscosity which is achieved when the shear rate approaches infinity, n is a parameter between 0 and 1, and λ_3 is a parameter which is assumed to be one.

The above equations are solved with the following initial conditions:

$$\mathbf{u}|_{t=0} = \mathbf{u}_0 \tag{6}$$

$$\mathbf{A}|_{t=0} = \mathbf{A}_0 \tag{7}$$

where $\mathbf{u}_0$ and $\mathbf{A}_0$ are the known initial values of the velocity and the configuration tensor.

The particle velocity $\mathbf{U}$ and angular velocity ω are governed by

$$M\frac{d\mathbf{U}}{dt} = M\mathbf{g} + \mathbf{F} \tag{8}$$

$$I\frac{d\boldsymbol{\omega}}{dt} = \mathbf{T} \tag{9}$$

$$\mathbf{U}|_{t=0} = \mathbf{U}_0 \tag{10}$$

$$\boldsymbol{\omega}|_{t=0} = \boldsymbol{\omega}_0 \tag{11}$$

where M and I are the mass and moment of inertia of the particle, and $\mathbf{F} = \circ(-p\mathbf{I} + \boldsymbol{\sigma}).\mathbf{n}\,ds$ and $\mathbf{T} = \circ(x - X)\times\left[(-p\mathbf{I} + \boldsymbol{\sigma}).\mathbf{n}\right]ds$ are the force and torque acting on the particle. Here X is the center of particle and the integral is over the particle surface. The particle density will be denoted by ρ_P. In this investigation we will assume that the particle is circular or spherical,

and therefore we do not need to keep track of the particle orientation. The particle position is obtained from

$$\frac{d\mathbf{X}}{dt} = \mathbf{U} \tag{12}$$

$$\mathbf{X}|_{t=0} = \mathbf{X}_0 \tag{13}$$

where X_0 is the position of particle at time t=0.

2.1 Dimensionless parameters

Next, we nondimensionalize the above equations by assuming that the characteristic length, velocity, time, stress and angular velocity scales are D, U, D/U, ηU/H and U/D, respectively. We will remove the hydrostatic pressure variation from p and add it to the buoyancy term in (8). It is easy to show that the non-dimensional equations after using the same symbols for the dimensionless variables are:

$$\mathrm{Re}\left[\frac{\partial \mathbf{u}}{\partial t} + \mathbf{u}.\nabla\mathbf{u}\right] = -\nabla p' + \nabla.\boldsymbol{\sigma} \qquad \text{in } \Omega\backslash\overline{P(t)}$$

$$\nabla\cdot\mathbf{u} = 0 \qquad \text{in } \Omega\backslash\overline{P(t)}$$

$$\frac{\partial \mathbf{A}}{\partial t} + \mathbf{u}.\nabla\mathbf{A} = \mathbf{A}.\nabla\mathbf{u} + \nabla\mathbf{u}^{T}.\mathbf{A} - \frac{1}{\mathrm{De}}(\mathbf{A} - \mathbf{I}), \qquad \text{in } \Omega\backslash\overline{P(t)}$$

$$\frac{\rho_P}{\rho_L}\mathrm{Re}\frac{h}{D}\frac{M}{\rho_P D^3}\frac{d\mathbf{U}}{dt} = -G\frac{h}{D}\frac{M}{\rho_P D^3} + \circ(-p'\mathbf{I} + \boldsymbol{\sigma}).\mathbf{n}\, ds$$

$$\frac{\rho_P}{\rho_L}\mathrm{Re}\frac{h}{D}\frac{I}{\rho_P D^5}\frac{d\boldsymbol{\omega}}{dt} = \circ(x - X)\times\left[(-p'\mathbf{I} + \boldsymbol{\sigma}).\mathbf{n}\right] ds \tag{14}$$

Here $\mathrm{Re} = \frac{\rho_L U D}{\eta}$ is the Reynolds number, $\mathrm{De} = \frac{\lambda_r U}{D}$ is the Deborah number, G $= \frac{(\rho_P - \rho_L)gD^2}{\eta U}$ is the gravity parameter, $\frac{\rho_P}{\rho_L}$ is the density ratio and p'=p-ρgh. For low Reynolds numbers the velocity scale for a sedimenting particle is given by U $= \frac{(\rho_P - \rho_L)gD^2}{\eta}$. When this characteristic velocity is used the parameter G reduces to one. In this case, the motion of a particle sedimenting near a wall depends on four independent

parameters: Re, De, h=H/D and $\frac{\rho_P}{\rho_L}$. The dimensionless parameters De and Re in this group may be replaced by the elasticity number E and the Mach number M.

2.2 Collision strategy

In our simulations we will assume that the lubrication forces are large enough to prevent the particle from touching the wall. The collisions between the particle and the domain walls are prevented by applying a body force that acts when the distance between the particle and a wall is of the order of the element size. This additional body force--which is repulsive in nature--is added to equation (8). The repulsive force between the particles and the wall is given by

$$\mathbf{F}_j^W = \begin{cases} 0 & \text{for } d > 2R + \rho \\ \frac{1}{\varepsilon_w}(\mathbf{X} - \mathbf{X}_j)(2R + \rho - d)^2, & \text{for } d < 2R + \rho \end{cases} \qquad (15)$$

where d is the distance between the centers of the particle and the imaginary particle on the other side of the wall Γ_j, $\mathbf{X}$ is the particle center, $\mathbf{X}_j$ is the center of imaginary particle and ε_w is a small positive stiffness parameter (see Figure 2). The above particle-wall repulsive forces are added to equation (8) to obtain

$$M\frac{d\mathbf{U}}{dt} = M\mathbf{g} + \mathbf{F} + \mathbf{F}'$$

where $\mathbf{F}' = \sum_{j=1}^{4} \mathbf{F}_j^W$ is the repulsive force exerted on the particle by the walls. In our simulations, ρ is equal to one and half times the velocity mesh size and $\varepsilon_w = 10^{-5}$. Notice that the repulsive force acts only when the distance between the particles is smaller than ρ. In our simulations, therefore, the particle cannot touch the walls. The distance of closest approach, however, can be decreased by refining the mesh.

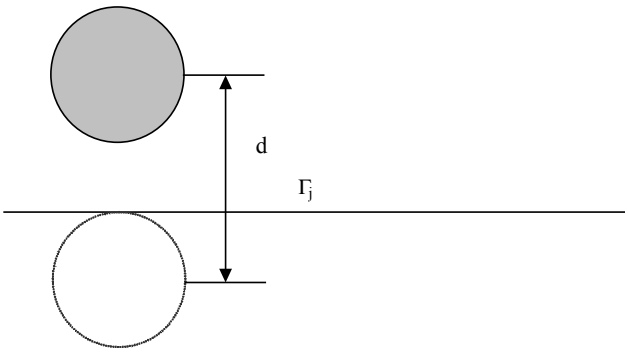

Figure 2. The imaginary particle used for computing the repulsive force acting between a particle and a wall.

2.3 Time discretization using the Marchuk-Yanenko operator splitting scheme

The initial value problem (32) is solved by using the Marchuk-Yanenko operator splitting scheme which allows us to decouple its four primary difficulties: the incompressibility condition, the nonlinear advection term, the constraint of rigid-body motion in $P_h(t)$, and the equation for the configuration tensor (see [13] for details). The operator splitting gives rise to the following four sub-problems:

1. The first step gives rise to a Stokes-like problem for the velocity and pressure distributions which is solved by using a conjugate gradient method [16].
2. The second step is a nonlinear problem for the velocity which is solved by using a least square conjugate gradient algorithm [16].
3. The third step is a linearized hyperbolic problem for the configuration tensor or stress. This problem is solved by using a third order upwinded positive only scheme [17,18]. The two key features of this scheme are: a positive only scheme that guarantees the positive definiteness of the configuration tensor, and a third order upwinding scheme for discretizing the convection term in the constitutive equation. These two features are important for obtaining a scheme that is stable at relatively large Deborah numbers.
4. The fourth step is used to obtain the distributed Lagrange multiplier that enforces rigid body motion inside the particles. This problem is solved by using a conjugate gradient method described in [14,15]. In our implementation of the method the flow inside the particles is forced to be a rigid body motion using the collocation method.

3. Results

In this section we discuss the numerical results obtained using the above algorithm for the motion of a particle sedimenting in a channel filled with Newtonian and Oldroyd-B fluids. We will assume that all dimensional quantities are in the CGS units. The parameter ρ in the particle-wall force models is equal to one and half times the velocity mesh size. For all test cases in this paper, the initial state of the stress and velocity in the fluid, and the particle velocity are assumed to be:

$$\mathbf{u}_0 = 0,$$

$$\mathbf{A}_0 = \mathbf{I},$$

$$\mathbf{U}_0 = 0,$$

$$w_0 = 0.$$

The initial value $\mathbf{A}_0 = \mathbf{I}$ implies that the Oldroyd-B fluid is in a relaxed state.

3.1 Sedimentation of a sphere in a channel

In this subsection we describe the motion of a sphere sedimenting near a wall in a channel filled with Newtonian and Oldroyd-B liquids. The channel cross-section is a square with sides 1.0 and the channel height is 4. We will assume that $\rho_L = 1.0$. The sphere diameter is 0.25, and thus the ratio L/D=4.0. In the Oldroyd-B model the parameter $c = \eta_p/\eta_s = 7$. We will consider both cases where the fluid is shear thinning and where the fluid viscosity is fixed. For a shear thinning fluid we will assume that $\eta_\infty = 0.1\eta_0$, λ_3=1.0 and n is equal to 0.25 or 0.8. The no slip boundary condition is applied along the box surface. The zero shear viscosity, the relaxation time and the shear thinning properties of the viscoelastic liquid are varied to understand their roles in the sphere's attraction towards the wall. In order to estimate the range of wall attraction, the sphere is dropped at several distances from the channel wall.

In our simulations the sphere is dropped near the right hand side channel wall, and in the middle of the front and back walls (see figure 1c). From this figure we note that the nearby channel wall is parallel to the yz-plane. The gravitational force acts along the negative z-axis. The anomalous sense of rotation is, therefore, along the y-axis, i.e., when viewed from the negative y-axis the anomalous rotation is in the clockwise direction. The angular velocity component along the y-axis is denoted by w. Also note that when the x-component of velocity u is positive the sphere moves towards the wall.

3.1.1 Convergence with mesh refinement

In order to show that our results converge with mesh size and time step refinements, we consider the case of a sphere sedimenting in an Oldroyd-B liquid with λ_r=5, η=0.008. The density difference $\rho_P - \rho_L = 0.00007$. The simulations are started by dropping a sphere at a distance of O(D) from the right hand side channel wall and at a height of 3.7. The Reynolds number for these simulations is ~0.49 and the Deborah number is ~0.32.

We have used two regular tetrahedral meshes to show that the results converge with mesh refinement. The number of velocity nodes and elements in the first mesh (M1) are 270641 and 192000, respectively. In the second mesh (M2), there are 68276 velocity nodes

and 375000 elements. The size of the velocity elements for the first mesh is 1/40, and for the second mesh is 1/50. The distance between the collocation points inside the sphere for the first mesh is ~1/40, and for the second mesh is ~1/50. The time step for these simulations is fixed, and assumed to be 0.005 or 0.002. These two time steps are selected to show that the obtained results are also independent of the time step.

From figure 3 we note that when the number of nodes used is approximately doubled the time evolutions the x-component of velocity u and the angular velocity w are approximately equal for t<~10 during which the sphere is in a state of downward acceleration. At t~10 the sphere reaches an approximate steady state after which u and w oscillate about a constant value. The results for t>~10 are sensitive to the mesh size and the time step. We may therefore conclude that for t<~10—the time duration for which the sphere is in a transient state—the results are independent of the mesh resolution. Similarly, a comparison of the curves marked "1" and "3" shows that when the time step is reduced by a factor of 2.5 for t<~10 the temporal evolutions of the particle velocity, the angular velocity, and also the trajectory do not change significantly. This shows that the results are also independent of the time step.

The Reynolds number based on the terminal velocity is ~0.49 and the Deborah number is ~0.32. The value of drag coefficient

$$Cd=\frac{\frac{1}{4}\pi D^2(\rho_p-\rho_L)g}{\frac{1}{2}\rho_L U^2 D}$$

is approximately 33.5 which is of the same order as the value for a sphere sedimenting in an infinite volume of Newtonian fluid. Here U is the sedimentation velocity. The drag coefficient for a sphere in a Newtonian liquid at Re=0.49 is ~30.

It is noteworthy that since the angular and linear velocities fluctuate slightly with time, the problem is not completely steady even in the frame attached to the particle, and therefore these results cannot be compared with well-known results for the flow past a fixed sphere. Simulations also show that the sphere rotates about the other two directions as well as slowly drifts along the y-direction. However, the angular velocity component about the y-axis is an order of magnitude larger and the velocity component along the y-direction is relatively small.

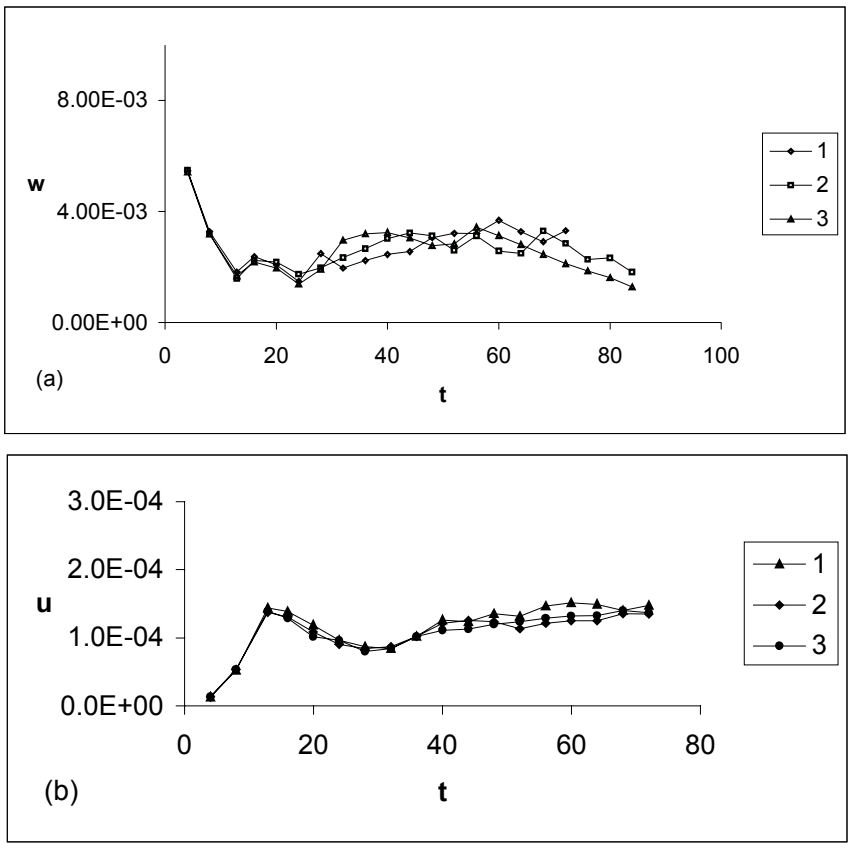

Figure 3. For a sedimenting sphere the time evolutions of w and u are shown. The Reynolds number is ~0.49 and the Deborah number is ~0.32. The sphere is dropped at h=0.8. (1) Using mesh M1 and the time step 0.005, (2) Using mesh M2 and the time step 0.005, (3) Using mesh M2 and the time step 0.002. The numerical results are approximately the same when the mesh size is decreased or when the time step is reduced.

3.1.2 Sedimentation of a sphere in a three-dimensional channel

We next investigate the case of a sphere sedimenting near a wall in a box filled with Newtonian and Oldroyd-B fluids. The simulations are started at t=0 by dropping a sphere at a distance of O(D) from the right hand side channel wall and at a height of 3.5. The parameters De and Re are varied by changing the fluid relaxation time λ_r, the fluid viscosity η, and the particle density.

In figures 4a-c we have shown the x-components of velocity u, the y-component of angular velocity w, the dimensionless distance h from the wall and the sphere height z as functions of time. For the Newtonian fluid η=0.008. For the Oldroyd-B fluid the relaxation

time is 10.0 and the zero shear viscosity is equal to the viscosity of Newtonian fluid. The density difference $\rho_P - \rho_L = 0.00007$.

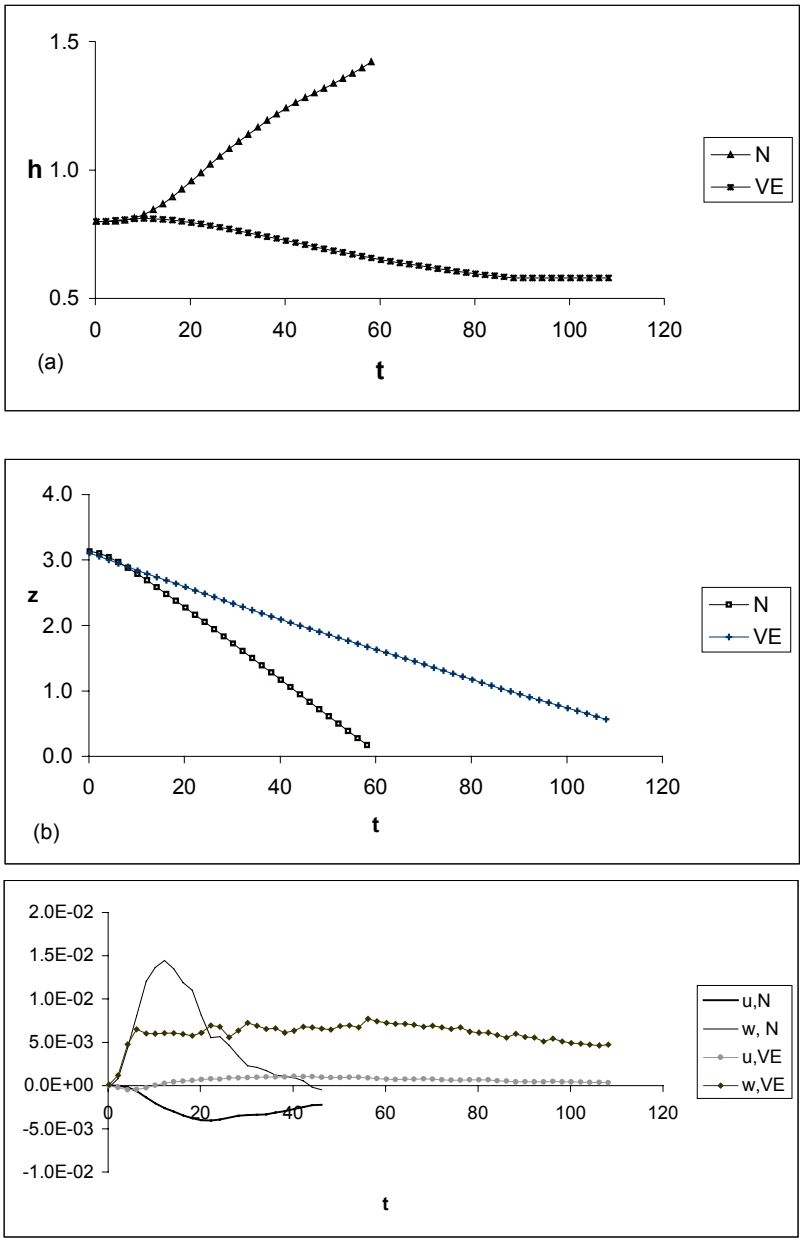

Figure 4. Sedimentation of a sphere in an Oldroyd-B liquids with λ_r=10, η=0.008 and $\rho_P - \rho_L = 0.00007$, and a Newtonian liquid with the same viscosity. The trajectories are shown for a sphere dropped at h=0.8. For the Oldroyd-B fluid Re ~0.71 and De ~0.90, and for the Newtonian fluid Re ~1.75. The curves for Newtonian liquid are denoted by N and that for Oldroyd-B liquid are denoted by VE. (a) The dimensionless distance from the wall h. Notice that the sphere sedimenting in the

Oldroyd-B liquid moves towards the wall, but in the Newtonian liquid it moves away from the wall. (b) The z-coordinate of the particle position. The figure shows that the sedimentation velocity in the Newtonian liquid is larger. (c) The x-component of velocity u and the angular velocity w are shown. The sense of rotation w is anomalous in both cases.

For t<~15, in both cases, the particle sedimentation velocity increases with time. In the Newtonian case after reaching a downward velocity of ~0.056, the sphere sediments with an approximately constant velocity. The Reynolds number based on this velocity is 1.75. In the viscoelastic case, on the other hand, a sedimentation velocity of ~0.0225 is reached. The Reynolds number is ~0.71 and the Deborah number is ~0.90. The Mach number is 0.79 and the elasticity number is 1.28.

Figures 4 a and c show that in the Newtonian case a sedimenting sphere released at h=0.8 drifts away from the wall. For t<20, the drift velocity u away from the wall increases in magnitude with time. After reaching a maximum value of 0.004, u decreases with time as the sphere moves away from the wall. The calculations were stopped when the sphere was close to the channel bottom. Also note that for this channel length the sphere did not reach a steady position in the channel cross section.

The initial velocity of a sphere released in the Oldroyd-B fluid at the same distance from the wall as above, i.e., h=0.8, is also away from the wall. But, as the viscoelastic stresses increase in magnitude with time, the velocity component normal to the wall changes sign and the sphere begins to move towards the wall. The time taken for the viscoelastic stresses to build-up is around 8 which is of $O(\lambda_r)$. From figure 4c we note that the velocity component towards the wall increases in magnitude with time and reaches an approximately constant value of 0.001 at t=~20. As the distance between the sphere and the wall decreases, both u and the sedimentation velocity slowly decrease with time. The body force of (15), which acts when the distance between the sphere and the wall is less than one and half times of the velocity element size, keeps the sphere from touching the wall. In our simulations, therefore, there is a minimum allowed distance between the sphere and the wall. The value of this minimum distance for simulations can be reduced by refining the mesh.

From figure 4c we note that when the sphere is close to the wall for both Newtonian and viscoelastic cases w is positive which means that the sense of rotation is anomalous. The

angular velocity in the Newtonian case decreases with time as the sphere moves away from the wall. In the Newtonian case a maximum angular velocity of ~0.014 radians/s is attained. In the viscoelastic case for t<7 the x-component of angular velocity increases with time and then it slowly decreases with time as the distance from the wall decreases. The maximum angular velocity is ~0.007 radians/s. For the viscoelastic case the angular velocity oscillates about the average value. The oscillations are a consequence of the relatively small magnitude of wD/2 compared to the sedimentation velocity. It is noteworthy that it was noted in [4] that for a sphere sedimenting in a viscoelastic liquid "the rotation rates are noisier but distinctively negative (anomalous)." In [4] the angular velocity was measured using an image-processing technique.

Figure 5b shows that when Re=~0.71 and De=~0.90 the velocity field around the sphere is not symmetric. From this figure we note that since w=~0.007 radians/s and the sphere is moving downwards at a speed of 0.0225, in a fixed frame the velocity on the sphere surface closer to the wall is larger than that on the surface away from the wall. Also note that in a frame moving with the sphere the stagnation points on the particle surface are shifted towards the wall. Therefore, based on the potential flow theory a net pressure force acts on the sphere away from the wall.

In figures 5b tr**A** distribution is shown at t=40 after the particle reaches its terminal velocity. The trace of configuration tensor is used to show the distribution of normal stresses; In the state of equilibrium tr**A** is 3 (in three-dimensions). Since all flows become viscometric at a solid wall, on the boundary of a solid particle the normal stress is zero and tr**A** is equal to $3 + 2\ (\dot{\gamma}\lambda_r)^2$, where $\dot{\gamma}$ is the shear rate at the wall. From figure 5b we note that tr**A** on the sphere surface away from the wall is larger than on the surface closer to the wall. Therefore, the shear rate on the former surface is larger than on the latter. If we assume that the normal stress on the sphere surface is given by $-\Psi_1(0)\dot{\gamma}^2$, as is the case for a second order fluid, the net normal viscoelastic stress contribution must act towards the wall. But, of course, for an Oldroyd-B liquid the normal component of extra stress is zero. Also note that the viscoelastic fluid around the particle takes a time of $O(\lambda_r)$ to relax back to the state of equilibrium. Since for our simulation De is ~0.9, there is a region behind the particle in which the viscoelastic stresses are relatively large.

3.1.3 Dependence on the initial distance from the wall

In this section we discuss the role of the initial separation between the sphere and the wall on the spheres trajectory. For four different values of the initial dimensionless separation h the time evolutions of the vertical position z and h are shown in figures 6 a and b. Simulations were stopped when the sphere reached a distance of approximately one diameter from the bottom. The parameters are the same as in figure 4. The approximate values of De and Re are 0.90 and 0.71, respectively.

From figure 6a we note that the sedimentation velocity decreases with decreasing distance from the wall, and thus the drag acting on the sphere increases as the sphere moves closer to the wall. Also, for all four cases h decreases with time (see figure 6b). But, for the sphere released at h=1.2 the approach towards the wall is much slower than for the sphere released at h=0.68. The figure clearly shows that the rate of approach towards the wall decreases with increasing initial distance from the wall. As noted above, in our simulations the minimum allowed distance between the sphere and the wall is approximately one and half times the velocity element size. For the spheres released at h=0.68 and 0.8 this minimum separation is reached before the sphere reaches near the bottom. But, for the initial separations of h=1.0 and 1.2 the sphere was away from the wall as it approached the bottom. From this figure we also note that the initial motion of the sphere for all cases is away from the wall. This, as noted above, is a consequence of the fact that the Newtonian behavior prevails for $t<\sim O(\lambda_r)$. After a time interval of $O(\lambda_r)$ the viscoelastic stresses become important and the sphere starts to move towards the wall. From figure 6c we note that u becomes positive earlier for the case where the initial separation from the wall is smaller.

From figure 6c we also note that the angular velocity w is positive for t>10, i.e., the sense of rotation is anomalous, for all four cases. The initial sense of rotation for h_0 =1.2, however, is normal and w decreases with decreasing separation from the wall.

Since for an initial separation h=1.0 the sphere did not come close to the vertical wall before reaching the bottom, we did calculations for this case in a domain which is assumed to be periodic in the z-direction. The time evolution of h is shown in figure 7a. In these calculations the sphere falls through the periodic domain three times. The approximate values of De and Re are 0.9 and 0.71, respectively. From this figure we note that initially h increases, i.e., the Newtonian behavior dominates, but then it starts to decrease with time as the

viscoelastic stresses become important. The rate of decrease of h increases with decreasing h until the sphere comes close to the wall. We may therefore conclude that a sphere dropped at h=1 also feels the wall attraction, but the vertical distance traveled before touching the wall is much larger. Actually, as we have seen above, even for an initial separation h=1.2 the sphere is attracted towards the wall, but the vertical distance traveled before touching the wall would be even greater.

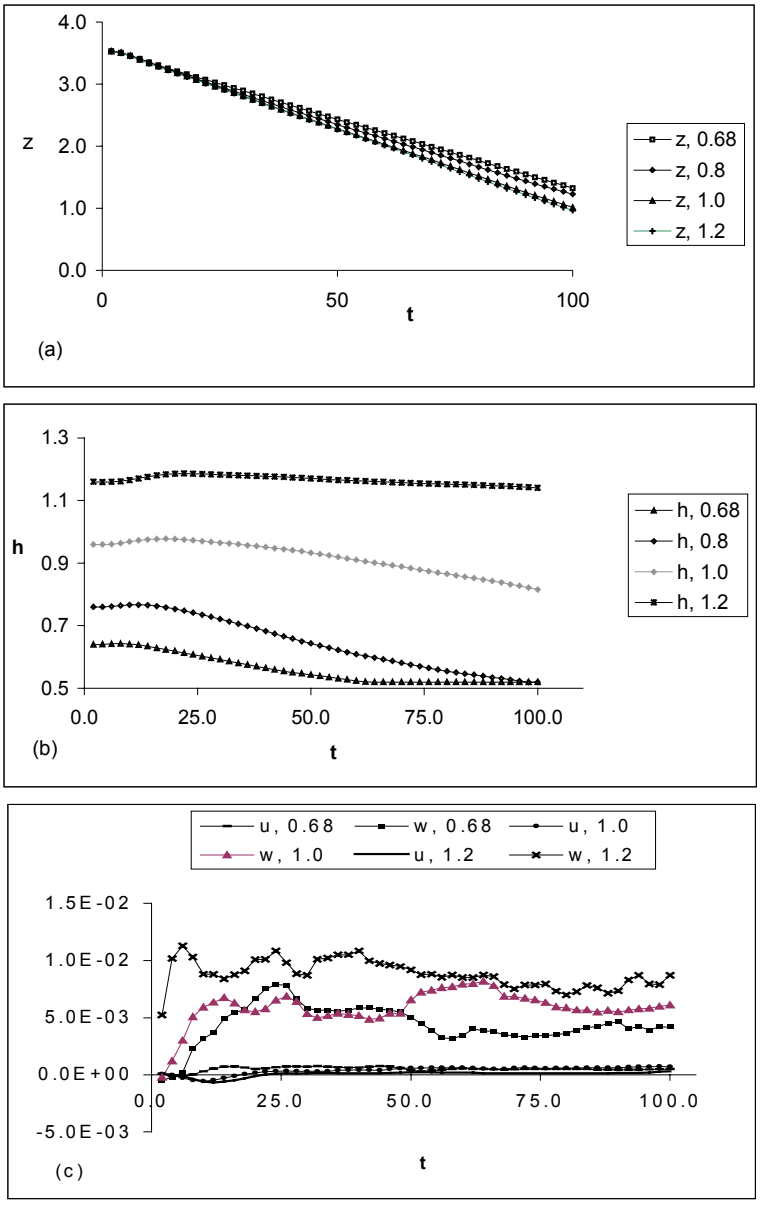

Figure 6. Sedimentation of a sphere in an Oldroyd-B liquids with λ_r=10, η=0.008 and $\rho_P - \rho_L = 0.00007$. The parameters Re~0.71 and De~0.9. The sphere is dropped at four different

values of the initial distance h=0.68, 0.8, 1.0 and 1.2. (a) The z-coordinate of the particle position is shown, (b) The dimensionless distance from the wall h is shown, (c) The x-component of velocity u and the angular velocity w are shown. Notice that when the initial position of the sphere is closer to the wall its sedimentation velocity is smaller and the velocity component towards the wall u is larger. The sense of rotation is anomalous and the magnitude of angular velocity decreases with decreasing distance from the wall.

In figure 7b the time evolution of h for a sphere dropped at h=1 in a periodic domain is shown for $\rho_P - \rho_L = 0.00002$ and η=0.26. The fluid relaxation time is 25. The approximate values of Re 0.024 and De is 0.23**.** From this figure we note that the sphere approaches the wall more slowly than for the Re=0.7 case discussed above.

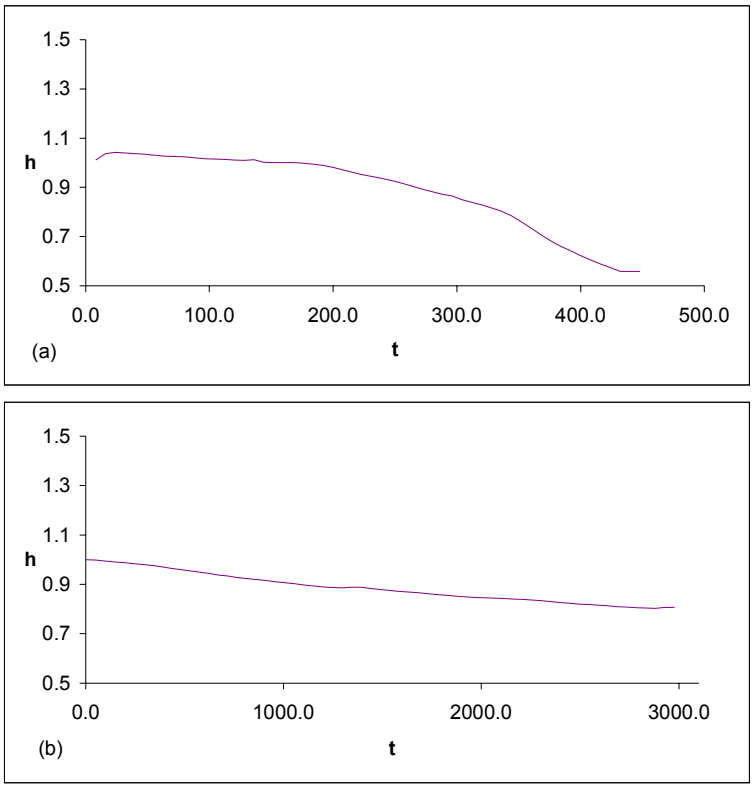

Figure 7. For a sphere dropped at h=1 in the Oldroyd-B fluids, the dimensionless distance h from the wall is shown. The domain is periodic along the z-direction. (a) Re=0.71 and De=0.9, $\rho_P - \rho_L = 0.00007$, (b) Re=0.024 and De=0.23, $\rho_P - \rho_L = 0.00002$. The sphere moves towards the wall, but the ratio of average u and sedimentation velocity U in (a) is approximately two times larger than in (b).

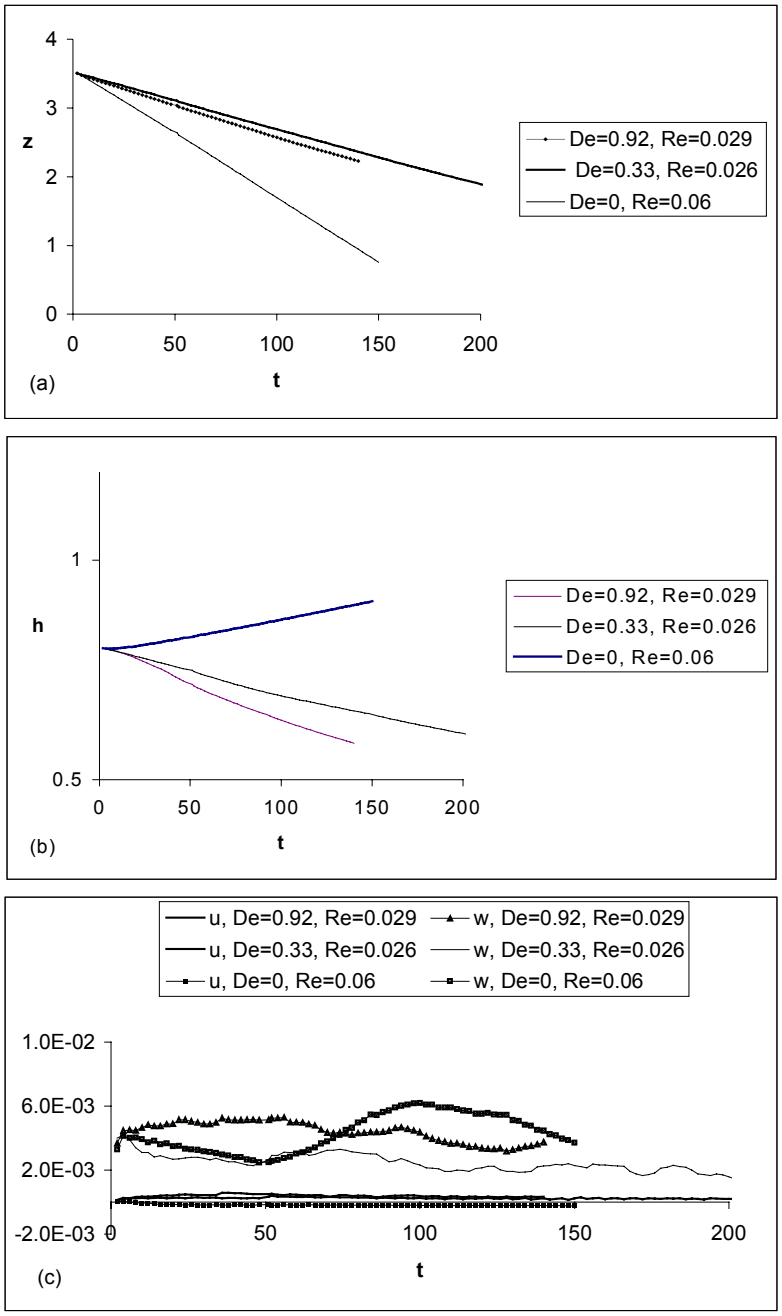

Figure 8. Sedimentation of a sphere dropped at h=0.8 in the Newtonian and Oldroyd-B liquids for η=0.08 and $\rho_P - \rho_L = 0.0001$ is shown. For the Oldroyd-B cases Re=0.026 and De=0.33, and Re=0.029 and De=0.92, and for the Newtonian case Re ~0.06. (a) The z-coordinate of the particle position is shown, (b) The dimensionless distance from the wall h is shown, (c) The x-component of velocity u and the angular velocity w are shown. The figure shows that both the rate of approach towards the wall and the angular velocity increase with increasing De. The sedimentation velocity is larger for the Newtonian liquid, as the sphere moves away from the wall.

These results are in good agreement with the experimental results [1-4] that for a given fluid-particle combination the particles dropped farther away from the wall travel longer vertical distances before touching the wall. This suggests that we may define a distance from the wall beyond which the wall attraction is negligible. The value of this distance, of course, depends on the fluid properties as well as on the diameter and density of the particle.

3.1.4 The role of Deborah number on the wall attraction

In figures 8a and b the vertical position z and the dimensionless distance from the wall h are shown as functions of time for a sphere sedimenting in Newtonian and Oldroyd-B fluids. The fluid viscosity η is 0.08 and the density difference $\rho_P - \rho_L = 0.0001$. The sphere is released at h = 0.8. The Reynolds number for the Newtonian case is 0.06, and for the two viscoelastic cases the Reynolds numbers are 0.026 and 0.029. The Deborah numbers for the two viscoelastic cases are 0.33 and 0.92. For the two viscoelastic cases the elasticity numbers are 12.7 and 31.7 and the Mach numbers are 0.093 and 0.16. From figure 8a we note that the sedimentation velocity is approximately equal for the two viscoelastic cases, but it is significantly larger for the Newtonian case. Clearly, since in the Newtonian case the sphere moves away from the wall, the influence of wall on the drag is weaker. Also note that the sedimentation velocity is slightly larger for the case with a larger value of De. This behavior of viscoelastic liquids is not unexpected [6]. For example, the drag coefficient of a cylinder placed in an Oldroyd-B fluid decreases with De for De <~O(1). But, for the higher values of De the drag coefficient increases with increasing De.

From figure 8b we note that for the two viscoelastic cases the sphere moves towards the wall, but for the Newtonian case it moves away from the wall. For both viscoelastic cases, the sphere reaches the wall before reaching the bottom. From figure 8c we note that the velocity component towards the wall u for De=0.92 is larger than that for De=0.33. In the Newtonian case the sphere did not reach an equilibrium position in the channel cross section before reaching the bottom. From figure 8c we also note that the sense of rotation for all three cases shown is anomalous, and that w for De=0.92 is larger than for De=0.33. For the Newtonian case the angular velocity first increases and then decreases as the particle moves away from the wall. Another important difference from the cases discussed in figure 6, where similar results are shown at a larger value of Re or a smaller value of the elasticity number E, is that the time interval for which the Newtonian behavior persists is smaller. As a

consequence the sphere has a little tendency to move away from the wall before the viscoelastic stresses become important.

In figures 9 a and b the vertical position z and h are shown as functions of time for a sphere sedimenting in the Oldroyd-B fluids for Re=O(1). The sphere is released at h= 0.8. The Reynolds number is 0.71, and the Deborah number is 0.46 and 0.90. From these figures we note that the sedimentation velocities for the two cases are approximately equal. The rate of drift towards the wall is however much larger for the case with a larger De. We may therefore conclude that the tendency of a sedimenting sphere to move towards the wall increases with increasing De, and that this behavior exists for the Reynolds number range investigated, i.e., for 0.02<Re<0.91.

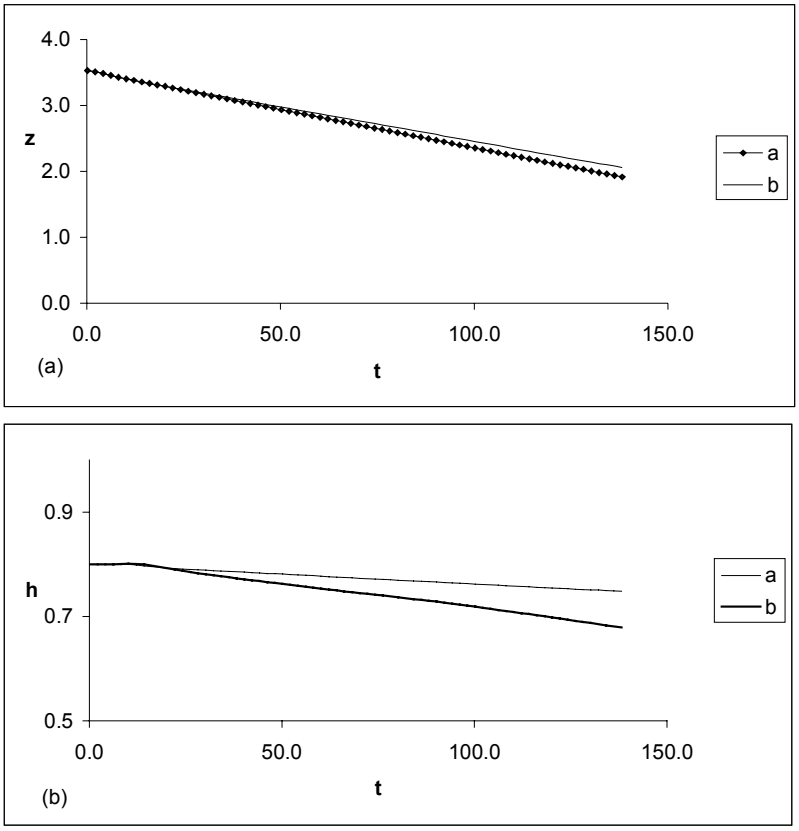

Figure 9. Sedimentation of a sphere dropped at h=0.8 in the Oldroyd-B liquids. The Reynolds number is ~0.71. For “a” De ~0.90 and for “b” De ~0.46. (a) The vertical position z is shown, (b) The dimensionless distance from the wall h is shown. The figure shows that both the sedimentation velocity and the ratio of average u and sedimentation velocity U, which is a measure of the rate of approach towards the wall, increases with increasing De.

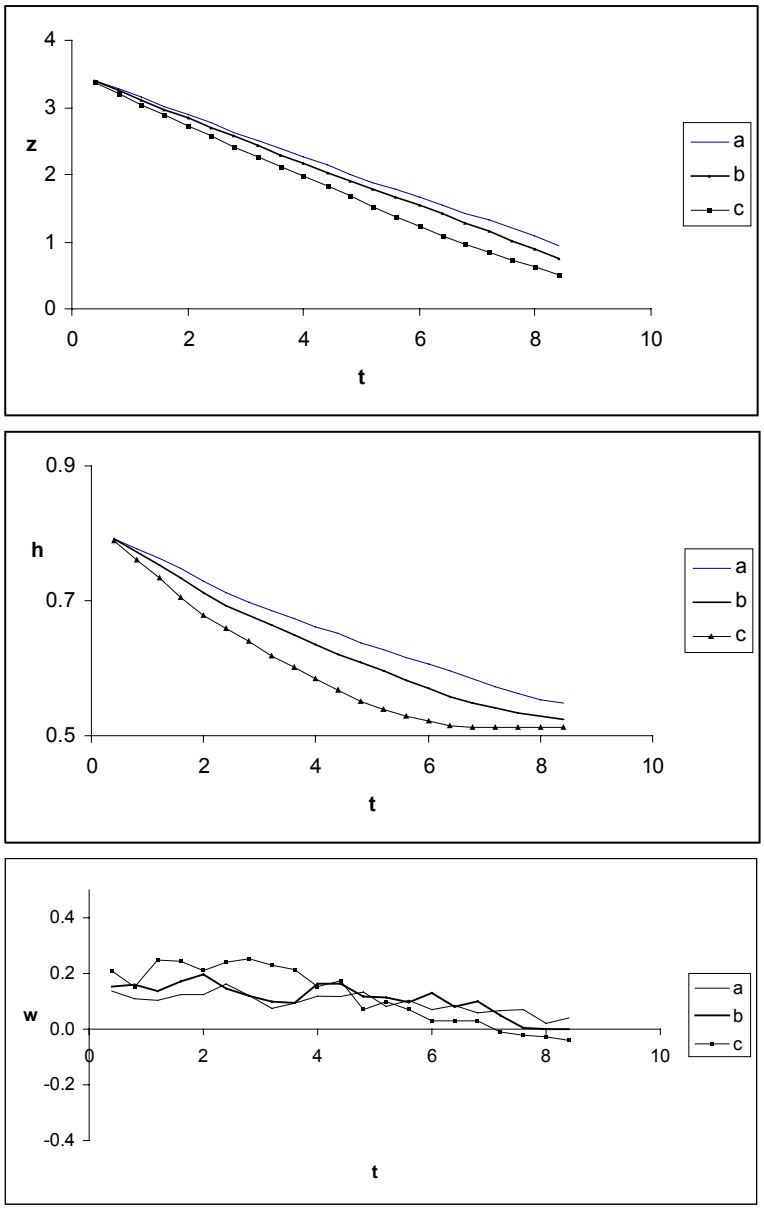

Figure 10. Sedimentation of a sphere in an Oldroyd-B liquids with λ_r=10, η=0.8 and $\rho_P - \rho_L = 0.04$ is shown. For "a" the viscosity is fixed. The shear thinning parameter n for "b" is 0.8 and for "c" is 0.25. The sphere is dropped at h=0.8. (a) The vertical position z is shown, (b) The dimensionless distance from the wall h is shown (c) The angular velocity w is shown. The figures show that the shear thinning enhances the velocity component towards the wall which is the largest for case (c). As expected, the shear thinning also causes an increase in the sedimentation velocity. The angular velocity is relatively insensitive to the shear thinning parameter n. Also notice that the angular velocity decreases as the distance between the sphere and the wall decreases and becomes slightly negative for case (c).

3.1.5 The role of shear thinning on wall attraction

In this section we discuss the role of shear thinning on the trajectory of a sedimenting sphere. We consider three cases: (a) fluid is not shear thinning, (b) shear thinning with n=0.8, and (c) n=0.25. The fluid with n=0.25 is more shear-thinning than with n=0.8. For all three cases, λ_r=10, and η =0.8 and $\rho_P - \rho_L = 0.04$**.** The Reynolds number based on the average sedimentation velocity for the three cases are 0.098, 0.103 and 0.121, respectively. The Deborah number for the three cases are 0.38, 0.40 and 0.46, respectively. The time evolutions of the vertical position z and h for these three cases are shown in figures 10 a and b. From the first figure we note that the sedimentation velocity is the largest for the case with n=0.25, which is expected as for a smaller value of n the fluid is more shear thinning.

From figure 10b we note that the shear thinning also changes the velocity component towards the wall. For all three cases shown the sphere moves towards the wall but the velocity towards the wall is the largest for n=0.25. The velocity towards the wall is the smallest for case (a) for which the viscosity is fixed. Since both sedimentation velocity and the velocity component towards the wall are different, it is interesting to look at the ratio of distance traveled in the x- and z-directions which is equal to tanθ, where θ is the angle between the sphere trajectory and the vertical wall. The angle θ can be used as a measure of the rate of approach towards the wall. The tanθ values for the three cases are 0.0246, 0.0291 and 0.035, respectively. Since tanθ is the largest for case (c), we may conclude that the shear thinning enhances the wall attraction of a sedimenting sphere. From figure 10c we note that the shear thinning does not have a significant influence on the angular velocity. The angular velocity w decreases with decreasing distance from the wall.

As noted earlier in section 1, for a second order fluid the viscoelastic contribution to the normal stress on the particle surface is compressive and its value is equal to $-\Psi_1(0)\dot{\gamma}^2$ [6,7]. It was shown in [9] that all flows become viscometric at a solid surface and argued that the shear thinning amplifies the effect of normal stresses. Specifically, for a given value of the wall shear stress, the shear rate must increase for a shear thinning liquid to maintain this fixed value of the shear stress. Consequently, the viscoelastic normal stresses, which are proportional to the square of shear rate, are larger for a shear thinning liquid. Our simulations support this argument as the shear thinning increases the rate of approach towards the wall.

3.2 Sedimentation of a cylinder in a two-dimensional channel

In this section we discuss the case of a cylinder sedimenting near a wall in a channel filled with Oldroyd-B and Newtonian fluids. The width of the channel is 2 and the height is 8. The no slip boundary condition is applied along the four channel walls. We will assume that for both Oldroyd-B and Newtonian fluids $\eta = 0.2$ and $\rho_L = 1.0$. For these 2D calculations the viscoelastic fluid is assumed be non shear-thinning. The cylinder diameter is 0.2. The simulations are started at t=0 by dropping a single particle at a distance of 0.2 from the channel right wall and at a height of 7.2. To perform simulations at different Deborah and Reynolds numbers the relaxation time λ_r is varied between 0.2 and 1 and the cylinder density is varied between 1.01 and 1.1.

We have used a regular triangular finite element mesh to discretize the domain. The particle domain is also discretized using a triangular mesh similar to the one used in [13]. The size of the velocity elements is 1/96, and the size of the particle elements is 1/70. There are 148417 velocity nodes and 73728 elements. The time step for these simulations is fixed, and assumed to be 0.0001. We have verified that the results are independent of the time step and the mesh resolution.

The time evolutions of z, h, and w for a cylinder sedimenting in Oldroyd-B and Newtonian fluids are shown in figures 11a-c. For the two Newtonian cases shown the sedimentation velocities are ~1.5 and 0.52, and the corresponding Reynolds numbers are 1.51 and 0.52. For the two viscoelastic cases the sedimentation velocities are ~1.17 and 0.37, and the Reynolds numbers are ~1.17 and 0.37. The Deborah numbers for the two cases are ~1.17 and 0.37. As noted above for a sphere, the sedimentation velocity of a cylinder in an Oldroyd-B fluid for De<~1 is smaller than that in a Newtonian liquid with the same viscosity and density, and therefore the Reynolds number for the Oldroyd-B fluid is smaller.

From these figures we note that when Re=O(1) and the particle is one diameter away from the wall, in both Newtonian and viscoelastic fluids, the direction of initial rotation is clockwise. But, as the sedimentation velocity increases, the direction of rotation reverses to counterclockwise, i.e., to a normal sense of rotation. For example, for Re=1.17 the particle rotates in the clockwise direction only for t<0.02. Also note that the magnitude angular velocity about the z-direction w decreases with decreasing Re. The sense of rotation changes when Re is O(0.1) or smaller. For example, for Re=0.13 and De=0.7 the average magnitude of

w is around 0.02 and the average direction of rotation is clockwise (see figure 11d). But, the angular velocity fluctuates about the mean value and even changes sign.

From figure 11 we note that for the range of Re and De investigated, a sedimenting particle moves away from the nearby vertical wall in both Newtonian and Oldroyd-B fluids. Also note that the velocity component away from the wall for the viscoelastic case is smaller than for the Newtonian case with the same viscosity. The stable position of the particle is somewhere between the channel centerline and the wall. The exact location of this stable position depends on the parameter values De, L/D, ρ_L/ρ_P and Re. These results are in agreement with those reported in [6].

It is interesting to note that for some parameter values the stable position may be less than one diameter away from the wall. For example, from figure 11d we note that a particle released at h=1 in the Oldroyd-B fluid move towards the wall. But, when in the same fluid it is released at h=0.7 it moves away from the wall. The stable position in this case is around h=0.83. In other words, when the cylinder is released between the stable position and the channel centerline it moves towards the stable position which for the first case is in the same direction as the channel wall. In a Newtonian fluid with the same viscosity the particle moves away from the wall (see figure 11d).

We wish to emphasize that for the parameter range investigated by us and in [6] the cylinder stays away from the wall in both Newtonian and Oldroyd-B liquids. On the other hand, when De=O(1) a sphere sedimenting in an Oldroyd-B fluid moves towards the wall and reaches a distance of less than one and half element size from the wall, where the body force (12) is applied to keep it away from the wall. In this sense, the motion of a sphere is different from that of a cylinder.

Figure 12a shows that when Re ~ 0.13 and De=0.65 the velocity field around the cylinder is not symmetric. Also note that since the particle is rotating in the clockwise direction with an angular velocity of 0.02 radians/s and moving downwards at 0.14 cm/s, in a frame moving with the particle the stagnation points on the particle surface are closer to the wall. Hence, based on the potential flow theory a pressure force acts on the particle away from the wall. Also, as noted above, for Re=O(1), the rotation is counterclockwise and thus the pressure force acts towards the wall, but the cylinder still moves away from the wall indicating that the viscous and elastic stresses are important in determining its trajectory.

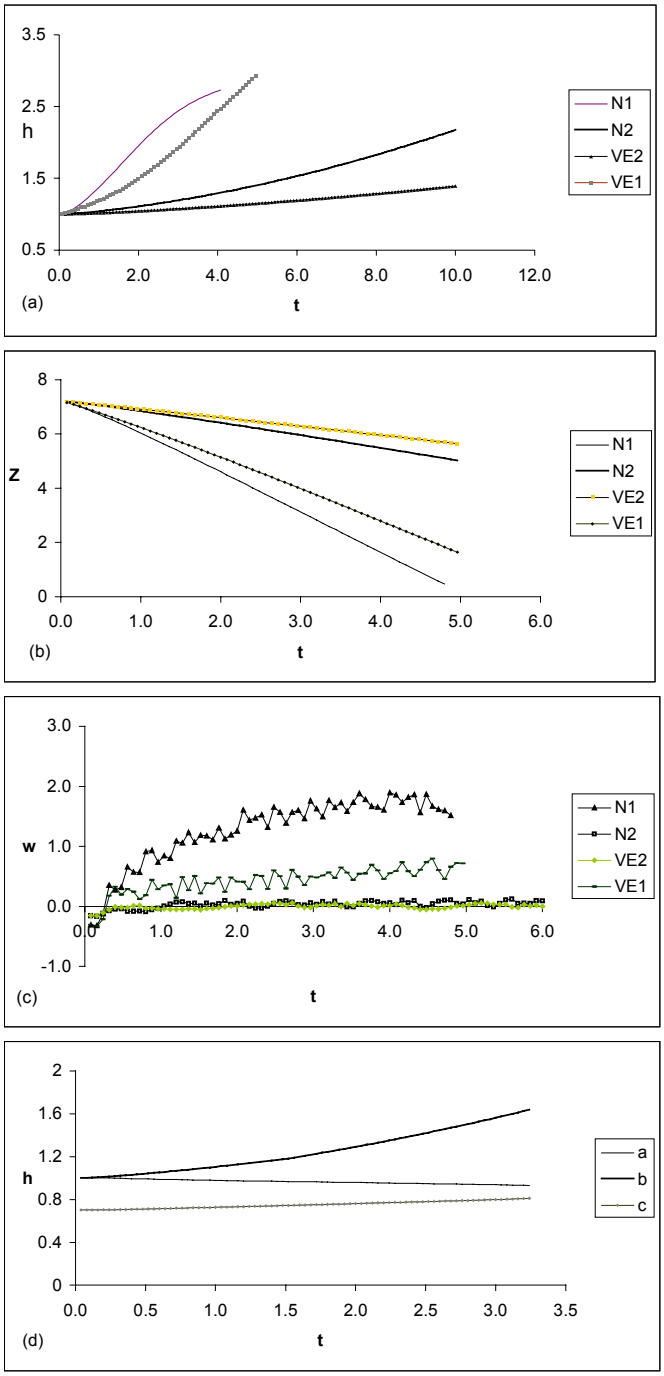

Figure 11. Sedimentation of a cylinder in Newtonian and Oldroyd-B liquids with η=0.2 is shown. For "N1" Re ~1.51 and $\rho_P - \rho_L = 0.1$; for "N2" Re ~0.52 and $\rho_P - \rho_L = 0.03$; for "VE1" Re ~0.37, $\rho_P - \rho_L = 0.03$ and De ~0.37, and for "VE2" Re ~1.17, $\rho_P - \rho_L = 0.1$ and De ~1.17. a) The vertical position z is shown, (b) The dimensionless distance from the wall h is shown, (c) The angular velocity w is shown, (d) The dimensionless distance from the wall h is shown for $\rho_P - \rho_L = 0.01$. For "b" Re=0.15 and for "a" and "c" Re= 0.13 and De=0.65.

From figure 12b we note that tr**A** is relatively large near the surface of the cylinder. The regions of large values of tr**A** near the particle surface merges together behind the particle and there is a region behind the particle in which the viscoelastic stresses are relatively large.

4. Conclusions

The distributed Lagrange multiplier/fictitious domain method [13] is used to study the motion of rigid particles sedimenting near a vertical wall in Newtonian and viscoelastic fluids. The viscoelastic liquid is modeled using a shear thinning Oldroyd-B model. The method is implemented using a combined weak formulation where the forces and moments between the particles and fluid cancel. The Marchuk-Yanenko operator-splitting technique is used to decouple the difficulties associated with the incompressibility constraint, and the nonlinear convection and viscoelastic terms. Simulations are performed in both two and three dimensions.

In three dimensions, simulations show that when the Deborah number based on the sphere velocity is O(1) and its initial position is close to the wall, it moves towards the vertical wall. This tendency to move towards the vertical wall is enhanced by an increase in De and by shear thinning. In a Newtonian liquid, on the other hand, the particle moves away from the vertical wall and attains a steady position between the channel center and the wall. Also, in a Newtonian liquid, the particle moves away from the wall whether or not the fluid shear thins. In simulations, the sphere is kept away from the wall by applying the body force (12) which acts when the distance between the sphere surface and the wall is smaller than one and half times the velocity element size. The direction of rotation of a sedimenting sphere when it is close to a vertical wall, for both Newtonian and viscoelastic liquids, is anomalous, i.e., the sphere rotates as if rolling up the wall. However, when the sphere is away from the wall the direction of rotation reverses. These results are in good agreement with the experimental results reported in [1-4].

In two dimensions, on the other hand, simulations show that a sedimenting cylinder moves to a stable position away from the wall. This happens in both Newtonian and Oldroyd-B liquids. The location of this stable position depends on the parameter values. For some parameter values, the stable position may be less than one diameter away from the wall, but for the parameter range investigated it is always away from the wall. These results prove that

the attraction between a sedimenting particle and the wall is a three-dimensional effect, i.e., exists for a sphere but not for a cylinder.

Acknowledgements

This work was partially supported by the National Science Foundation KDI/New Computational Challenge grant (NSF/CTS-98-73236), by the US Army, Mathematics, by the DOE, Department of Basic Energy Sciences, by a grant from the Schlumberger foundation and from Stimlab Inc. and by the Minnesota Supercomputer Institute.

5. References

[1] D.D. Joseph, Y.J. Liu, M. Poletto and J. Feng, Aggregation and dispersion of spheres falling in in viscoelastic liquids. *J. Non-Newtonian Fluid Mech*. **54** (1994), 45-86.

[2] Y.J. Liu, J. Nelson, J. Feng and D.D. Joseph, Anomalous rolling of spheres down an inclined plane, 50(1993), 305-329.

[3] D.D. Joseph, J. Nelson, H. Hu and Y.J. Liu, Competition between inertial pressures and normal stresses in the flow induced anisotropy of solid particles. P. Moldenaers and R. Keunings (Eds.). Theoretical and Applied Rheology. Elsevier, Amsterdam, 1992, pp 60-65.

[4] D.L.E. Becker, G.H. McKinley and H.A. Stone, Sedimentation of a sphere near a plane wall: weak non-Newtonian and inertial effects. *J. Non-Newtonian Fluid Mech*. **63** (1996), 45-86.

[5] A.J. Goldman, R.G. Cox and H. Brenner, Slow viscous motion of a sphere parallel to a plane wall. I. Motion through quiescent fluid, *Chem. Eng. Sci.* 22, (1967) 637-651.

[6] D.D. Joseph and J. Feng, A note on the forces that move particles in second-order fluid. *J. Non-Newtonian Fluid Mech*. **64** (1996), 299-302.

[7] D.D. Joseph, Flow induced microstructure in Newtonian and viscoelastic fluids. *In Proc. 5th World Congress of Chem. Engng, Particle Technology Track, San Diego. July 14-18. AIChE* **6** (1996), 3-16.

[8] J. Feng, P.Y. Huang, and D.D. Joseph, Dynamic simulation of sedimentation of solid particles in an Oldroyd-B fluid, *J. Non-Newtonian Fluid Mech*. **63** (1996), 63-88.

[9] P.Y. Huang, H.H. Hu and D.D. Joseph, Direct simulation of the sedimentation of elliptic particles in Oldroyd-B fluids, *J. Fluid Mech*. **362** (1998), 297-325.

[10] D.D. Joseph and Y.J. Liu Orientation of long bodies falling in a viscoelastic liquid. *J. Rheol.* **37** (1993), 961-983.

[11] P.Y. Huang, J. Feng, H.H. Hu and D.D. Joseph, Direct simulation of the motion of solid particles in Couette and Poiseuille flows of viscoelastic fluids, *J. Fluid Mech*. **343** (1997), 73-94.

[12]H. Binous and R.J. Phillips, The effect of sphere-wall interactions on particle motion in a viscoelastic suspension of FENE dumbbells, *J. Non-Newtonian Fluid Mech*. **85** (1999), 63-92.

[13]P. Singh, D.D. Joseph, T.I Hesla R. Glowinski, and T.W. Pan, A distributed Lagrange multiplier/fictitious domain method for particulate flows. *J. Non-Newtonian Fluid Mech.* **91** (2000), 165-188

[14]R. Glowinski, T.W. Pan, T.I Hesla and D.D. Joseph, A distributed Lagrange multiplier/fictitious domain method for particulate flows. Int. J. of Multiphase Flows. **25** (1998), 201-233.

[15]R. Glowinski, T.W. Pan and J. Periaux, A Lagrange multiplier/fictitious domain method for the numerical simulation of incompressible viscous flow around moving rigid bodies, *C.R. Acad. Sci. Paris* **324** (1997), 361-369.

[16]M.O. Bristeau, R. Glowinski & J. Periaux, Numerical methods for Navier-Stokes equations. Application to the simulation of compressible and incompressible flows, *Computer Physics Reports* **6**, 73 (1987)

[17]P. Singh and L.G. Leal, *Theoret. Comput. Fluid Dynamics* **5** (1993)**,**107-137.

[18]D.D. Joseph, Fluid dynamics of viscoelastic liquids. (1990) Springer-Verlag, New York.